AD-A096 625 TEXAS UNIV AT AUSTIN F/G 7/4
AUGER ELECTRON SPECTROSCOPY AS APPLIED TO THE STUDY OF THE FRAC--ETC(U)
1980 M SCHMERLING, D FINELLO, H L MARCUS N00014-78-C-0094
UNCLASSIFIED NL

1 OF 1
AD A 096625

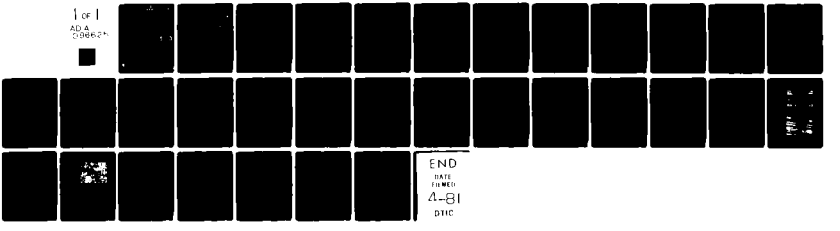

END
DATE FILMED
4-81
DTIC

[To be published in Scanning Electron Microscopy, 1981]

Auger Electron Spectroscopy as Applied to the Study of the Fracture Behavior of Materials

Contract N00014-78-C-0094

1980

33

Michael Schmerling, Duane Finello and H.L. Marcus
Mechanical Engineering/
Materials Science and Engineering
The University of Texas
Austin, Texas 78712

Abstract

This paper will describe the use of AES in a wide range of fracture problems. Included will be fracture studies of iron, aluminum based alloys and metal matrix/ceramic composites. The paper will also describe how the AES analysis is combined with the SEM, inert ion sputtering, SIMS, ESCA, and other surface and near surface tools to assist in determining the fracture behavior of materials in various environments.

Auger Electron Spectroscopy as Applied to the Study of the Fracture Behavior of Materials

Michael Schmerling, Duane Finello and H.L. Marcus
Mechanical Engineering/
Materials Science and Engineering
The University of Texas
Austin, Texas 78712

Introduction

One of the earliest applications of Auger Electron Spectroscopy (AES) in materials research was the study of the grain boundary fracture of steels[1-4]. The approaches used in these studies have been refined, but the research in fracture still follows the experimental approaches defined then. The major instrumental advance in AES made during the early stages was the improved spatial resolution associated with the development of the scanning Auger microscope[4-5]. The ability to get Auger data from areas less than the grain diameter in metals and ceramics allowed chemical details associated with the fracture process to be studied in detail. The transition during the last decade of the AES Microscope from a research laboratory instrument to one used routinely in most laboratories has tremendously broadened its application to studies of fracture and failure in a wide variety of applications.

It is the purpose of this review paper to describe the recent AES research being performed to develop an understanding of the fracture behavior of structural materials. The paper will draw heavily from the research efforts of the authors during the last few years.

The results will be presented from two viewpoints. The first will be the positive results obtained where AES clarified the fracture mechanisms. The second will be a discussion of the experimental problems associated with interpreting the AES data. In addition experiments using AES combined with SIMS, SEM and ESCA will be discussed.

Technical approaches:

There are two types of fracture problems associated with AES. The first is the problem where only a thin layer, several monolayers in extent, controls the fracture process. Included in this is the large class of problems related to grain boundary and interface segregation. In this case if the fracture surface is exposed to ambiant conditions for as short a period as a few minutes (prior to being put into a hard vacuum), the oxide formed and aerosol contamination will prevent the gathering of meaningful AES results on the interface

chemistry[1-3]. For this reason the sample must be fractured in situ in a hard vacuum, a clean hydrogen or an inert gas environment. The hard vacuum system should be baked prior to the fracture process to reduce the residual concentration of water vapor which quickly contaminates the fresh active metallic fracture surfaces in cases such as for aluminum and iron alloys. The baking is not as essential for fracture studies of ceramics and semiconductor materials.

The sample in the vacuum chamber can then be fractured under impact loading[2], torsion loading[3] or tensile loading[6]. The sample can be fractured over a range of temperatures by using either a cooling or heating stage. The AES analysis of the surface is then performed using the submicron electron beam. A schematic of a fracture arrangement is given in Figure 1. To enhance crack formation on the specific weak interface, fracture can be induced under either cyclic or sustained loading in an aggressive environment such as hydrogen[7-9]. This technique may allow the exposure of interfaces for AES analysis which would normally not fracture. Other techniques such as introducing embrittling elements by electrolytic charging followed by diffusion down the grain boundary have been tried with limited success. The

objective is to diffuse sufficient embrittling elements such as S or As down the interface to induce interface failure. The hypothesis is that the original interface chemistry will not be modified and will be measured during the in situ fracture and AES analysis.

The second type of fracture problem approached is one where the fracture is formed external to the system and AES analysis of the preexisting fracture surfaces is then obtained. In this case the important information must be composed of a layer much thicker than the contamination layers. An example of this type of study describes the combined use of AES and ESCA to evaluate stress corrosion cracking[10]. The oxide chemistry associated with the stress corrosion process gives clues to the origin of the fracture. Similar studies are in progress aimed at using AES and ESCA to distinguish between oxides such as Fe_2O_3 and Fe_3O_4 to determine the origin of critical preexisting flaws. In both these cases the oxides are very thick compared to the expected contamination layers. Another approach is the fracturing of a sample in an environment bearing an isotope of the element of interest. A combined AES and SIMS analysis to examine the environmental influence on fatigue crack growth using deuterium and O^{18} isotopes will be described later.

In all of the experiments described a vital aspect of the experiment is the combination of inert ion sputtering with the AES, SIMS and ESCA measurements to determine not only the chemistry of the fracture interface but the relative position of this interface to the rest of the structure of the materia.. An example of the applicabilitiy of this approach is in the interface fracture associated with metal-matrix composites. The fracture path is very sensitive to the existing layered structure associated with the composite. This will be discussed in more detail in the following section.

Fracture Studies

During the past 12 years AES has been used in many fracture studies. We will not attempt to delineate all of the studies but will focus on the recent work of the authors as being representative, but by no means uniquely representative of the recent AES fracture studies.

AES Studies of Grain Boundary Embrittlement in Steels

Since early this century it has been observed that low alloy steels can become embrittled if they are kept in a well defined (~350-575°C) temperature range over

extended periods of time. This "reversible temper embrittlement" consists of an increase in the ductile-to-brittle transition temperature for the steel; i.e., intergranular brittle failures occur at temperatures where the steel is used rather than only at very cold temperatures. The effect can be reversed by short anneals above 600°C.

Typical compositions for these steels are 0.4 wt% C, 3.5% Ni, 1.7% Cr and $\leq$ 0.06% Sn, P, or Sb (the balance being Fe). When embrittled alloys are fractured at room temperature, the fracture path is generally at prior austenite grain boundaries. This is also true for binary alloys of iron and some elements. The grain boundaries have been examined with AES after the specimens were fractured in a vacuum[2,3,7,11-19]. Concentrations of the trace elements S, P, Sn, Sb, As, Te, Se, Pb at the grain boundaries, sometimes orders of magnitude higher than in the bulk, were measured at the boundaries in different alloys. Significantly higher grain boundary concentrations of Ni, Si, Cr and other alloying elements were also found in these alloy systems. In almost all cases inert ion sputtering showed the depth of the increased concentrations to be from ~.5 to 1 nm for the trace elements but apparently two to three times as great for the alloying elements such

as Ni. Based on the AES and inert ion sputtering data several theories have been proposed to account for how a one or two monolayer region with high trace element concentration occurs and how one can account for microscopic fracture along it. One problem with the data is how to explain the observed differences in depth of the trace and alloying elements.

Plotting the concentration of Sn and Ni on a fractured grain (analyzing spot ~5000 nm) of an embrittled 3.5% Ni - 1.7% Cr - 0.4% C - 0.06 wt.% Sn steel versus sputter time, showed both elements having an approximately exponential decrease. The characteristic depth was two times as large for Ni as for Sn. To evaluate if the observed profile represented an actual physical difference in thickness, Sn and Ni were deposited from a Sn wetted Ni filament inside the Auger system in a submonolayer film on top of a grain previously sputtered to the bulk concentration[20]. Resputtering reproduced the same profiles observed on the original fractured specimen. It thus appears that Ni is more strongly bonded to the predominantly Fe matrix than Sn and is removed more slowly by sputtering leading to an apparent but artificial double thickness of the Ni rich region at the grain boundary when compared to the Sn layer

thickness, as illustrated in Figure 2. This can lead to significant errors in modeling the diffusion and fracture process.

AES Studies of Metal Matrix Composites

Auger microscopy has become an essential tool in the study of metal-matrix/ceramic fiber composite materials. In a fiber composite the maximum mechanical properties can usually be obtained by having all the fibers aligned in a single direction in the matrix material. Unfortunately, in directions normal to this unique axis the material is often weaker than the homogeneous matrix material. This occurs because the interface region between the fiber and the matrix is generally weaker than either one and the fracture path includes the interface[21].

In studies of Ti-6Al-4V matrix with B_4C/B or SiC fibers, fiber composites in the form of consolidated wires with the fiber axis in the plane of the plate were fractured inside of the AES vacuum system. The fracture paths, Figure 3, contain a large amount of interface and followed the fiber sides of the interface through the carbides as

determined from the characteristic carbon Auger derivative peaks. Careful peak shape studies can help determine which carbide, such as Ti or Si carbides in the SiC fiber composite, is present. Carbides and oxides near the SiC fibers and borides near the B_4C/B fibers along with S and Cl impurities were localized at the interface as determined by sputter profiling. The brittle compounds associated with these elements and their poor bonding to the adjoining phases created a layer that resulted in the lowest energy fracture path.

When samples of the same Ti-6Al-4V/SiC material were thermally cycled between 550°C and 40°C in air for nine days the fracture path was partially through degraded interfaces filled with oxides. No significant amount of carbide was found in the fracture interface. This degradation of the interface reduced the longitudinal fracture strength.

Similar studies with aluminum matrix/graphite fiber composites have indicated oxides, carbides and TiB_2 present at the fracture interface. To identify from Auger data what compound is present in an unknown sample, the spectra from a standard sample observed under identical conditions should be compared to the unknown. Both peak-to-peak heights and peak shape must be correlated. If the unknown was sputtered, the same parameters must be used on the standard to avoid any preferential sputtering modifications.

For example, a TiB_2 powder standard resulted in a direct correlation with the Auger data from the interface of the aluminum graphite composites.

An absolute check on compounds at the interface in Al/graphite fiber composites was made by correlating Auger data with a TEM study. Interfaces were isolated by either dissolving the matrix (in HCl, HCl-methanol mixture, or KOH) or by electropolishing the matrix away (in perchloric acid, ethanol and glacial acetic acid electrolyte). Small pieces of interface remained attached to the fibers. These were observed in the TEM. Diffraction patterns confirmed the presence of TiB_2 as well as oxides of aluminum and other minor component elements of the matrix. Al_4C_3 and TiC were also detected from the diffraction patterns. The difficulty of indexing polycrystalline electron diffraction patterns was lessened considerably by having the Auger data on the thin interface material[23].

In order to examine the basic structure of the Al-graphite interface and factors that influence the interface strength a model system was examined. Single crystal graphite flakes obtained from Ticonderoga granite were used. Since the basal plane of graphite is parallel to the plane of the flake, clean surfaces could be exposed by "peeling" off layers of graphite from the flake. In

vacuums ranging from $4x10^{-7}$ torr to $2x10^{-3}$ torr aluminum was deposited on the clean flake from an Al coated hot filament. The resulting oxide layer at the graphite-aluminum interface ranged from ~3nm (determined by sputter profiling) for the high vacuum case to ~20 nm for the low vacuum. When segments of the aluminum were peeled away from the flake and both newly exposed surfaces examined with AES, it was apparent that the fracture path was in the graphite for the thin oxides (a good interface bond) but partly through the oxides and partly through the graphite for the thicker oxides (a presumably weaker bond). In addition to the AES peel studies, electrical I/V characteristics were measured and interpreted using the AES results. Figure 4 shows the experimental arrangement[23].

AES of Fracture in Cast Iron

The morphology of the graphite particles in cast iron plays a major role in the fracture behavior of the iron[24]. Ductile iron has spheroidized graphite particles. Fracture takes place along the graphite-metal interface. AES has been performed to attempt to identify why the interface was the preferred path. The chemistry of the interface was found to be the controlling factor

in determining the morphology of the graphite, but the chemical composition apparently played no role in the fracture process. The fracture strength was controlled by the microstructure of the matrix[25-27]. In this case the AES results did not lead to an improvement in fracture properties but were of value in determining the process by which the fracture controlling graphite morphology was determined. Figure 5 is an example of the fracture surface of ductile iron.

AES/SIMS Study of Fatigue Crack Growth in Aluminum Alloys

The influence of gaseous environments on fatigue crack growth in structural alloys has been extensively studied over the years[28-30]. The AES/SIMS studies described here were aimed at looking at the transport of the embrittling species into the metal in the vicinity of the crack tip during the fatigue process. The study included gaseous H_2, D_2, D_2O, O_2, O_2^{18}, H_2O^{18}, N_2, Ar and hard vacuum as the environments for aluminum alloys fatigued in an environmental chamber. To separate the hydrogen and oxygen contamination, deuterium and oxygen-18 isotopes were used as the active environments. The samples were then examined in the AES/SIMS system with

the normalized results shown in Figure 6. The O^{18} as determined with SIMS is much deeper into the surface than the atmospheric oxygen as measured with AES and represents the oxide formed during fatigue. This oxide is thicker than one formed after fatiguing in vacuum. The deuterium is transported to a much greater depth[31-32] than the oxide. The shape of the deuterium profile can be explained as diffusion taking place after the fatigue crack growth process is complete. This was confirmed with examination of ion implantated deuterium profiles as a function of time[32].

Electron and Ion Beam Damage Influence on AES Analysis on Fractured Carbon Composites

In an attempt to determine the local bonding in the carbon fiber-metal matrix composites detailed AES spectrum analyses from the fracture surfaces were attempted. This section will describe the problems associated with detailed Auger peak analysis using graphite as an example.

Surfaces which contain carbon in any of a variety of forms (i.e., hydrocarbons, functional oxycarbon groups and highly graphitic carbons) are highly susceptible to perturbations in physical structure under electron beam exposure. These changes in initial surface structure are directly associated with changes in the carbon Auger peak shape, as in the case of single crystal graphite[33].

The changes undergone are permanent and may proceed through stages as the surface atoms approach a more disordered state. Electron-induced decomposition and selective desorption of other elemental species can occur in weakly bound carbonaceous compounds, rendering surface analysis impractical via electron beam techniques.

In order to minimize surface damage, x-ray photoelectron spectroscopy (XPS) is advantageous in surface analysis of graphite fibers, although the spatial resolution limitations of XPS make it unsuitable for many other applications in materials science[36]. Likewise, ion-induced surface damage occurs upon inert ion sputtering of graphite fibers, resulting in further perturbations in the carbon Auger peak shape (see Figure 7). It is noteworthy that no electron-induced local changes in secondary electron yield are visible following argon sputtering of graphite fibers, whereas such changes are apparent prior to sputtering.

Characteristic loss spectroscopy (CLS) can be used to obtain matrix-sensitive information concerning a surface[37-40]. This technique is considerably more delicate by virtue of the fact that it requires only a small fraction of the primary electron current density and voltage required with AES. The CLS process does not generate core holes; rather, it is intended to probe energy loss mechanisms experienced by backscattered

electrons which have undergone interactions with the uppermost surface layers of the specimen matrix.

CLS is accomplished by using an electron energy analyzer to measure the energy distribution of electrons backscattered from a surface subjected to a monoenergetic primary beam of electrons. Typically, the primary electron beam energy is set below 2000 eV because most Auger peak energies of interest lie below this energy. Ideally, with the primary beam held at the energy of an Auger peak, the response function obtained through CLS serves as a description of the changes in energy which analyzed electrons have undergone due to kinetic events unrelated to bonding. The response function is valid over an energy range of several hundred electron volts, so a single Auger peak can theoretically be deconvoluted with the CLS spectrum of the same range of analyzed energies.

Before discussing deconvolution further, an illustration of CLS data for graphite fibers will be given. With an electron beam of only a few picoamperes rastered over an area of a few hundred thousand square microns, it is possible to delay the onset of surface damage for several minutes. (For comparison, beam currents greater by more than four orders of magnitude are required to

obtain Auger data). The CLS spectrum in the initial state is presented in Fig. 8(a), somewhat different from the final state displayed in Fig. 8(b). The difference is that the latter exhibits a small plasmon peak adjacent to the elastic backscatter peak, visible because the carbonyl and lactone oxygen surface groups[34,35] have been decomposed by the electron beam. While performing AES on graphite fibers, the electron beam desorbs the weakly bound oxygen almost completely.

Traditionally, AES data handling has been facilitated by digital signal processing[41,42]. Routine application of deconvolution techniques[43-47] would be impractical without on-line access to a high-speed computer. Raw AES data is initially taken in analog form. Accurate digitization of the signal is a necessity in order to determine the existence of peak shifts and preserve peak shape. The digital energy increments should be discrete in terms of electron volts.

Superimposed upon the raw AES data is the large secondary electron background. It has been determined[48] that adjustment of an analytical function can simulate the background adequately over an energy range of a few hundred electron volts. Hence, the background

can be synthesized and subtracted from an Auger peak. After subtracting the background from an Auger peak in derivative form, integration is performed in order to prepare the measured data for deconvolution.

Once the corresponding derivative CLS data is digitized and integrated, it is desired to deconvolute matrix and instrumental effects from the integral Auger data using the integral characteristic loss data as a response function. The iterative deconvolution scheme[43] is accurate provided that the data contains relatively little fine structure so that the algorithm leads to convergence. Figure 9 compared the original integral Auger data from pyrolytic graphite with a reconvolution of the final deconvoluted result to ensure that the two match one another. Due to electron-induced surface damage caused by the primary electron beam, the carbon Auger peak from any type of graphite will not reproducibly characterize the form of carbon as anything different from pyrolytic graphite. Even graphite single crystal basal plane surfaces do not regularly produce the sharp structural features in peak shape that have been reported[33].

Carbides, however, do not possess the graphitic resonant bond character, and will tend to retain their physical structure by resisting electron-induced surface damage somewhat. Well-resolved carbon Auger peaks for several general carbide standards which exhibit noticeable differences have been reported[33]. Deconvoluted spectra of graphite and aluminum carbide are different (see Figure 10). The carbide peak has a sharper structure and this might be indicative of a more orderly surface structure.

The net result is that very little detailed information about the nature of the bonding at the fracture surface is obtainable with AES. In reality the fractured bonds have already undergone a major modification from the bonding in the original unfractured solid during the fracture process. The electron and ion beam damage makes it even more difficult to do any analysis.

It also should be noted that weakly bound elements such as Cl, Br, I etc. can easily be removed or greatly reduced in concentration by the electron beam before an AES analysis of the fracture surface is performed.

Summary

This review paper has tried to show, with a limited set of examples, how AES combined with other surface

sensitive tools can be used in studies of the fracture of materials. The applicability is widespread and routine in many laboratories. It was also pointed out that unless care is taken the observed data interpretation could have large errors. With care AES is a powerful tool for the study of fracture.

Acknowledgements

The authors acknowledge the support of this research by the Office of Naval Research, Contract N00014-78-C-0094. We appreciate the discussion with Dr. Swe-Den Tsai, and Anna Zurek, Deepak Mahulikar and Young Park, on their published and unpublished research.

References

1. L.A. Harris, J.A.P. 39, (1968) p. 1419.

2. H.L. Marcus, P.W. Palmberg, Trans AIME 245, (1969) p. 1664; ASM Trans Quart. 62 (1969) p. 1016.

3. D.F. Stein, A. Joshi and R.P. LaForce, ASM Trans. Quart. 62 (1969) p. 776.

4. N.C. Mac Donald, in Scanning Electron Microscope Symp. 4th Proc., O. Johari, editor (1971) pp. 89-96.

5. N.C. Mac Donald, H.L. Marcus and P.W. Palmberg in Scanning Electron Microscope Symp. 3rd Proc., O. Johari, editor (1970) pp. 25-31.

6. R.D. Moorehead, Rev. Sci. Instrum. 47 (1976) p. 455.

7. C. Briant, Corrosion 36 (1980) p. 497.

8. R.P. Wei, P.S. Pao, R.G. Hart, T.W. Weir and G.W. Simmons, Met. Trans. 11A (1980) p. 151.

9. R.P. Wei and G.W. Simmons, Scripta Met. 10 (1976) p. 153.

10. A. Joshi, Stress Corrosion Cracking, J. Yahalon and A. Aladjen Editors, Freund Publishing House, Tel-Aviv (1978).

11. C.J. MacMahon, Jr., Mat. Sci. & Eng. 42 (1980) pp. 215-226.

12. C. Lea, M.P. Seah and E. Hondros, Mat. Sci. & Eng. 42 (1980), pp. 233-244.

13. D.J. Dingley and S. Biggin, Phil. Trans. R. Soc. Lond. Series A 295 (1980) 165.

14. G.J. MacMahon, Jr., Mat. Sci. & Eng. 42 (1980) 215.

15. M. Guttman, Phil. Trans. R. Soc. Lond. Series A 295 (1980) 169.

16. M Guttman, Mat. Sci. & Eng. 42 (1980) 227.

17. J.P. Hirth, Phil. Trans. R. Soc. Lond, Series A 295 (1980) 139.

18. M.L. Jokl, J. Kamela, C.J. McMahon, Jr. and V. Vitrek, Met. Sci. (1980) 375.

19. J.P. Stark and H.L. Marcus, Met. Trans 8A (1977) pp. 1423-1430.

20. M. Schmerling, D. Finello and H.L. Marcus, Scripta Met 14, (1980) 1135.

21. J.A. Cornie and F.W. Crossman, Editors, Failure Modes in Composites, AIME-TMS (1977).

22. D.S. Mahulikar, Y.H. Park and H.L. Marcus, in Proceedings of US-Greece Symposium on Mixed Mode Crack Propagation, G. Sih and P.S. Theocaris, editors (1980).

23. S.D. Tsai, PhD Dissertation, The University of Texas, December 1980.

24. Sourcebook on Ductile Iron, American Society for Metals (1977).

25. W.C. Johnson and B.V. Kovacs, Met. Trans 9A (1978) 219.

26. W.B. Johnson and H.B. Smart, Met. Trans 8A (1977) 553.

27. J. Smith, L. Brown and H.L. Marcus, AFS Transactions (1980) 427.

28. M.R. Louthan, Jr. and R.P. McNitt, Editors, Environmental Degradation of Engineering Materials, Virginia Tech Printing (1977).

29. O.F. Devereux, A.J. McEvily and R.W. Staehle, Editors, Corrosion Fatigue, NACE, Houston (1972) 346.

30. M. Meshii, Editor, Fatigue and Microstructure, American Society of Metals (1979).

31. A.K. Zurek, H.L. Marcus, J.N. Cecil and R. Powers, Met Trans 11A (1980) 1920.

32. A.K. Zurek and H.L. Marcus, Proceedings of the SIMS-II Second International Conference on SIMS, San Francisco, August 1979.

33. C.C. Chang, in Characterization of Solid Surfaces, P.F. Kane and G.G. Larabee, editors, Plenum Press, NY (1974) chapter 20.

34. F. Hopfgarten, Fiber Sci. and Technol 12 (1979) 283.

35. F. Hopfgarten, Fiber Sci. and Technol 11 (1978) 67.

36. D. Finello and H.L. Marcus in Electron and Positron Spectroscopies in Materials Science and Engineering, O. Buck and H.L. Marcus, editors, Academic Press, NY (1979) pp. 121-181.

37. M.L. Knotek and J.E. Houston, Phys. Rev. B 15 (1977) 4580.

38. J.E. Rowe, J. Vac.Sci. Technol. 13 (1976) 798.

39. T.S. Sun, J.M. Chen, R.K. Viswanadham and J.A. Green, Appl. Phys. Lett. 31 (1977) 580.

40. J.J. Ritsko and M.J. Rice, Phys. Rev. Lett. 42 (1979) 666.

41. J.T. Grant, M.P. Hooker and T.W. Haas, Surf. Sci. 46 (1974) 672.

42. J.T. Grant, M.P. Hooker and T.W. Haas, Surf. Sci. 51 (1975) 318.

43. J.E. Houston, J. Vac. Sci. Technol. 12 (1975) 255.

44. M.A. Smith and L.L. Levenson, Phys. Rev. B 16 (1977) 2973.

45. J.A. Tagle, V. Martinez-Saez, J.M. Rojo and M. Salmeron, Surf. Sci. 79 (1978) 77.

46. C.J. Powell, Sol. State Comm. 26 (1978) 557.

47. H.D. Hagstrum and G.E. Becker, Phys. Rev. B 4 (1971) 4187.

48. E.N. Sickafus, Rev. Sci. Instrum. 42 (1971) 933.

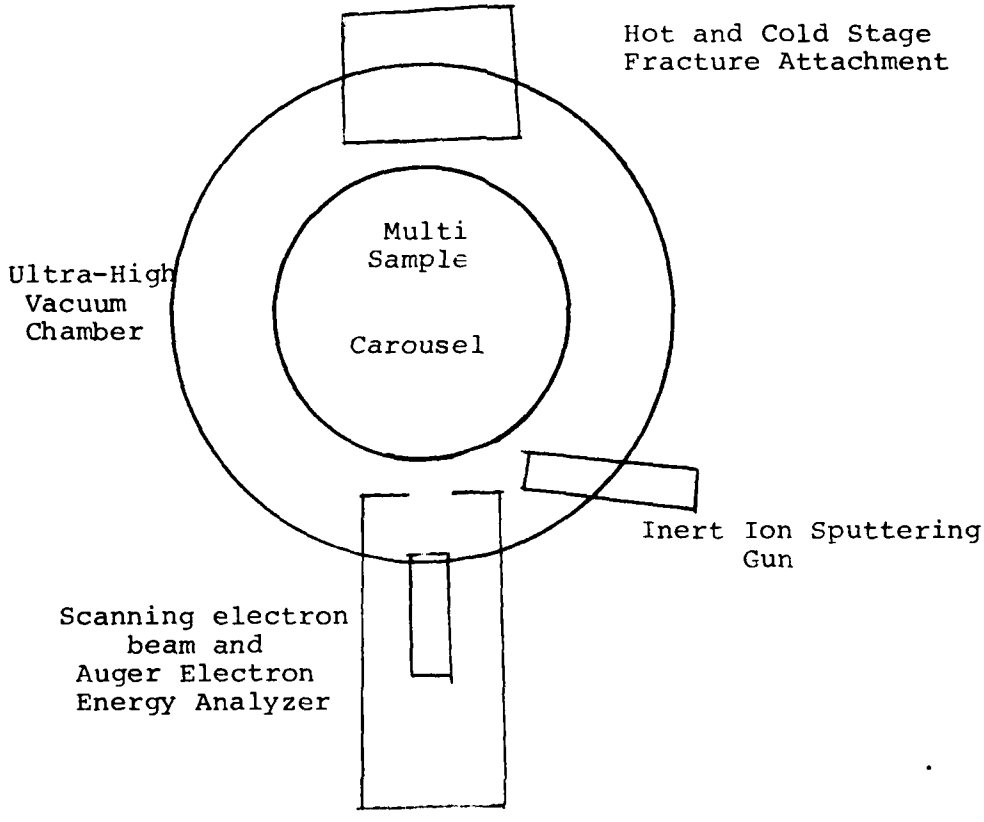

FIGURE 1

Schematic of Fracture Arrangement

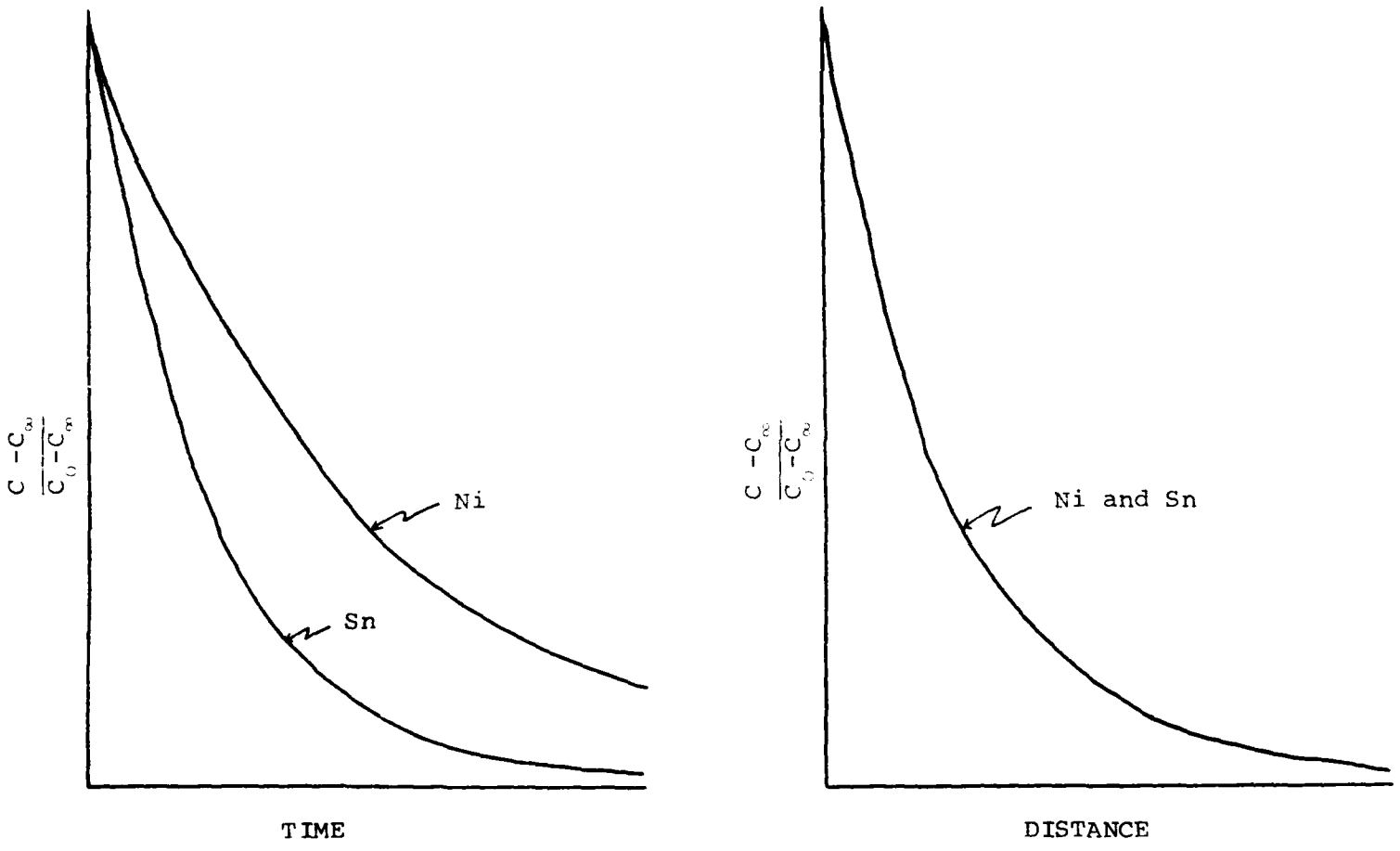

FIGURE 2

Schematic of normalized concentration of segregated Sn and Ni as detected by argon ion sputtering into an embrittled low alloy steel fracture surface

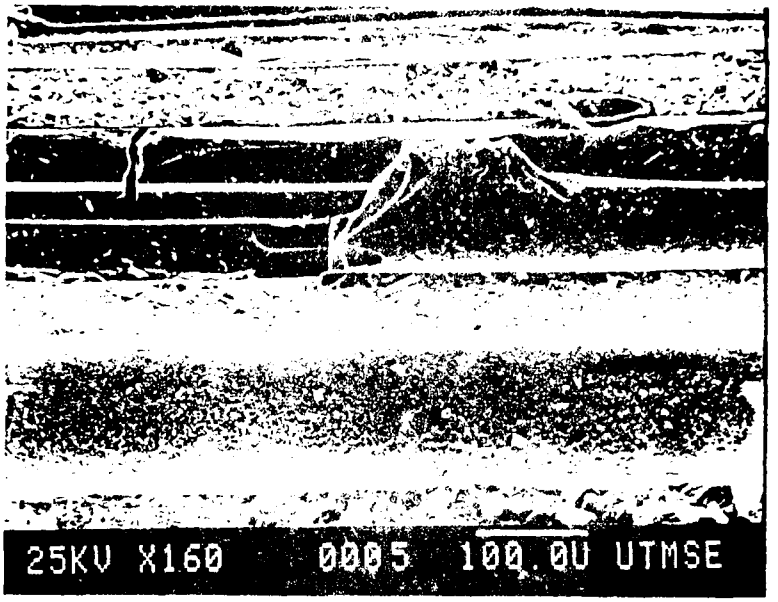

FIGURE 3 (a) Fracture surface of "Ti-6Al-4V/Cu" composite showing path through interface

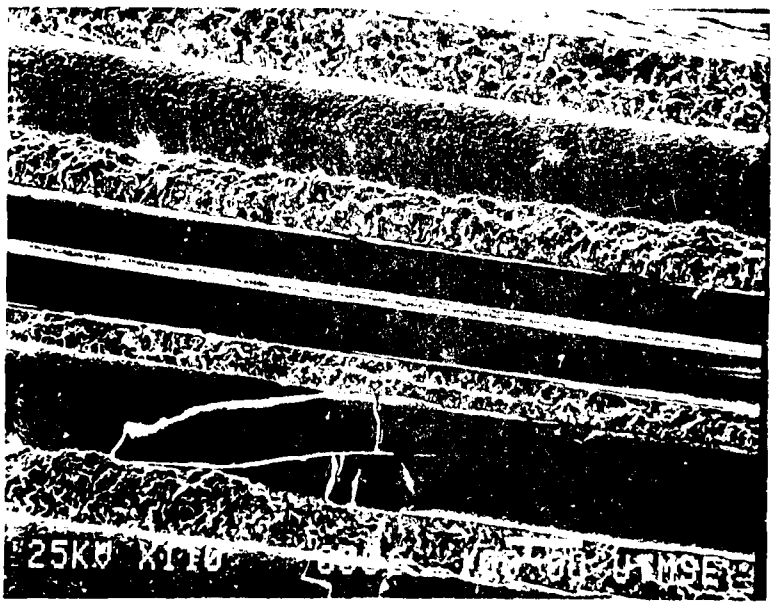

FIGURE 3 (b) Fracture surface of Ti-6Al-4V/B_4C/B composite

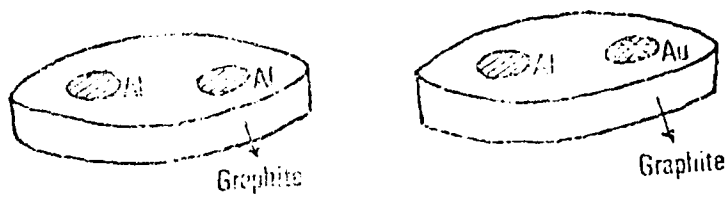

FIGURE 4 (a) Geometry of Al/Gr contacts for I/V measurements and peel tests.

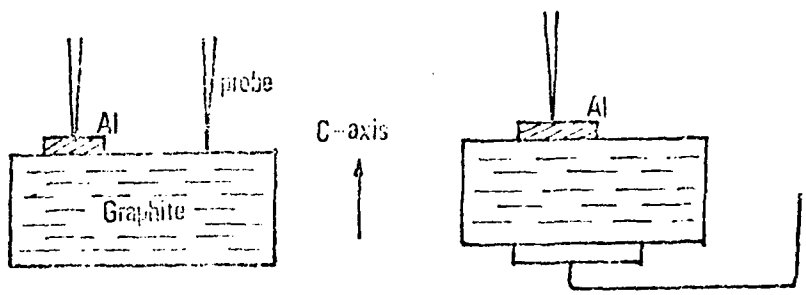

FIGURE 4 (b) Two types of contact configuration.

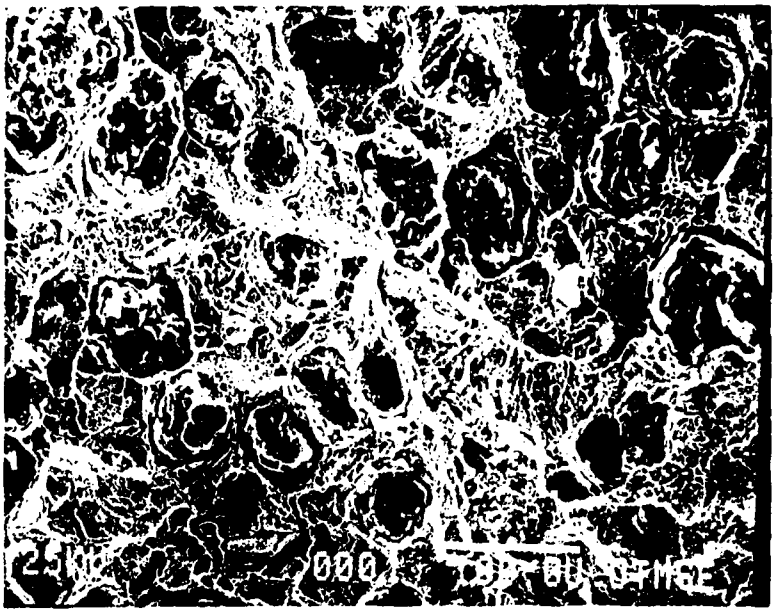

FIGURE 5

SEM of Fracture Surface of Ductile Iron.

FIGURE 7

Carbon Auger Features of Highly
Graphitic VSO-054 Fibers
(a) As Received and (b) After Sputtering

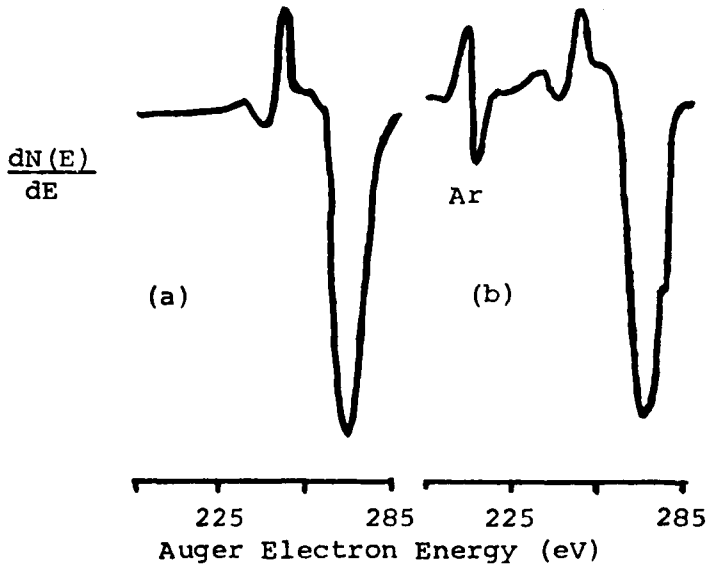

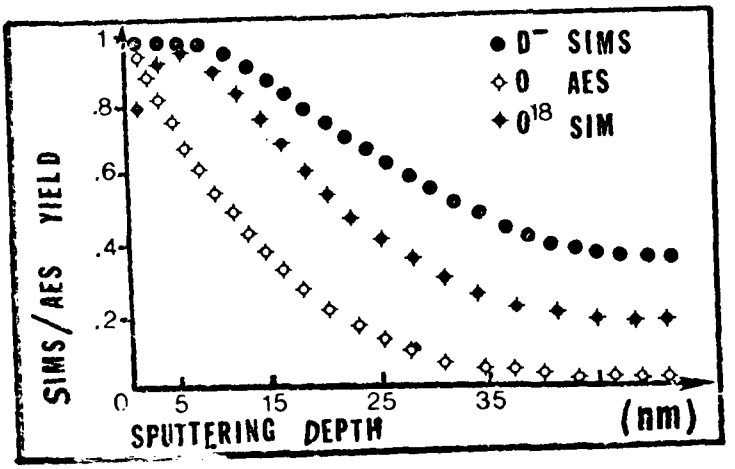

FIGURE 6

Sputter profile of deuterium and O^{18} as determined by SIMS and Oxygen determined by AES.

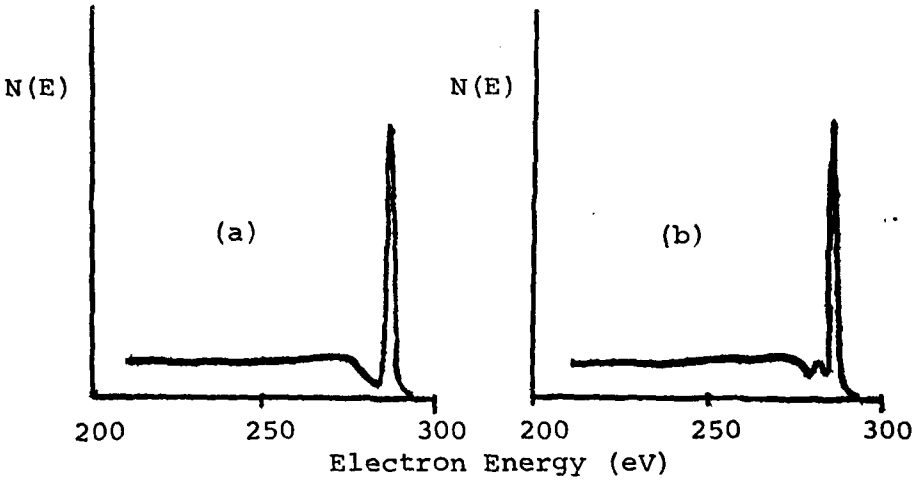

FIGURE 8. Integral characteristic loss spectra for high modulus pitch precursor type VSB-32 graphite fiber. Spectrum (a) represents the situation prior to extensive electron beam damage to the surface while spectrum (b) represents the heavily damaged surface exhibiting a small plasmon peak.

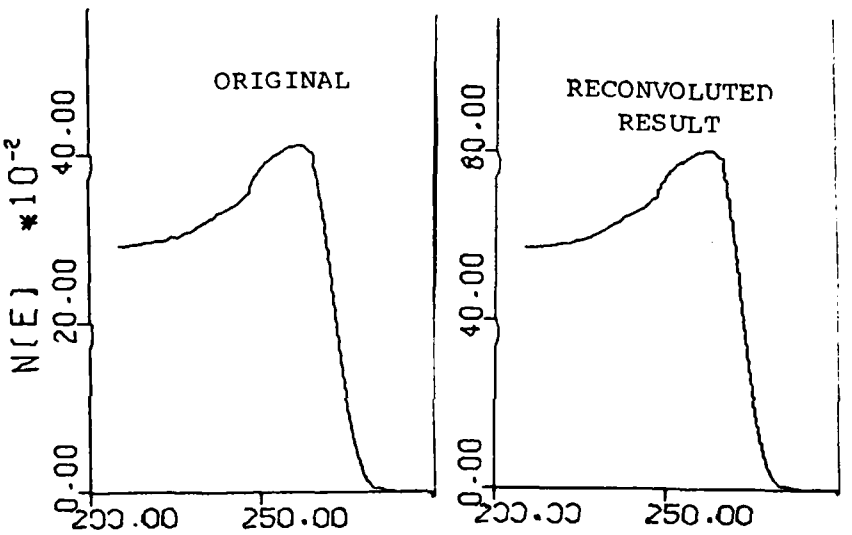
ORIGINAL
RECONVOLUTED
RESULT
N[E] *10⁻²
40.00
20.00
0.00
80.00
40.00
0.00
200.00
250.00
200.00
250.00
ELECTRON ENERGY (eV)

FIGURE 9

FIGURE 10

DECONVOLUTED SPECTRA

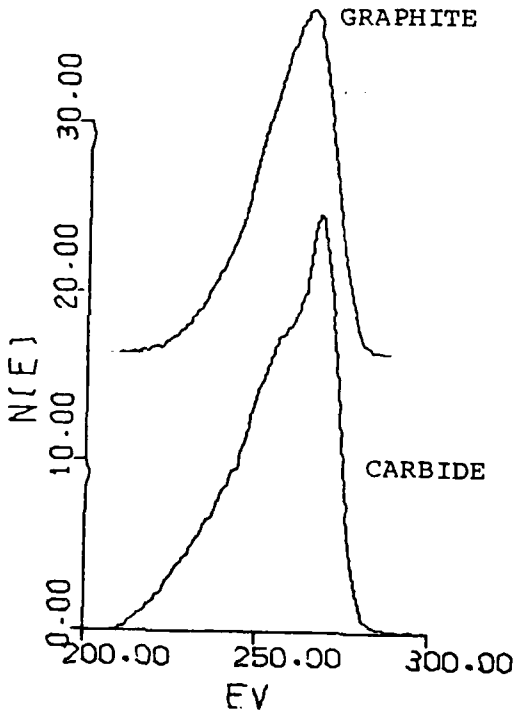

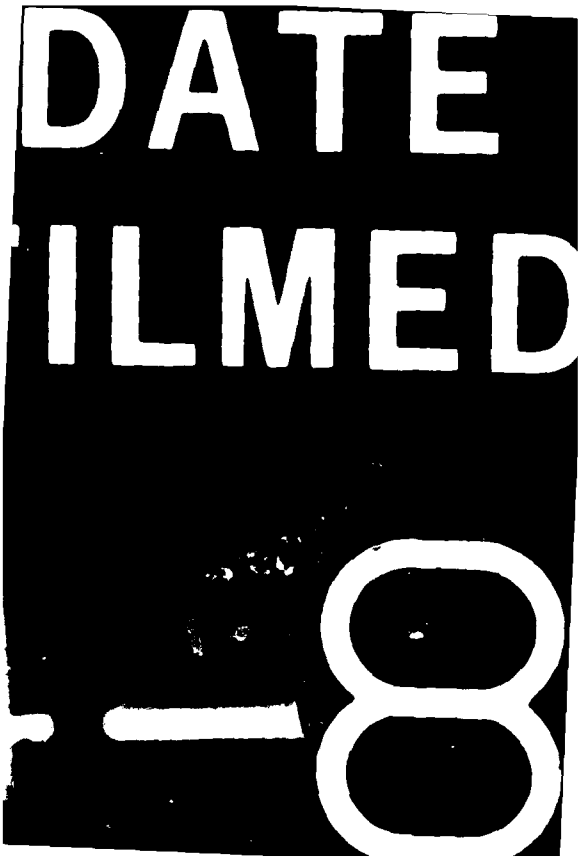
DATE
ILMED
8